SUPPLEMENTARY INFORMATION

Ca^{2+}-induced Movement of Tropomyosin on Native Cardiac Thin Filaments Revealed by Cryo Electron Microscopy.

Cristina Risi[1], Jamie Eisner[1], Betty Belknap[1], David H. Heeley[2], Howard D. White[1], Gunnar F. Schröder[3,4] and Vitold E. Galkin[1]

[1] Department of Physiological Sciences, Eastern Virginia Medical School, Norfolk, VA 23507, USA

[2]Department of Biochemistry, Memorial University, St. John's, NL, Canada A1B 3X9

[3] Institute of Complex Systems ICS-6, Forschungszentrum Jülich, 52425 Jülich, Germany

[4] Physics Department, Heinrich-Heine Universität Düsseldorf, 40225 Düsseldorf, Germany

SI Materials and Methods

Cryo EM sample preparation. We found that both the Tpm and Tn-complex partially dissociate from the TFs upon freezing and that the loss of these components of the TF depends on the blotting conditions. Large sample volumes (>3 µL) and long blotting times (> 5 sec) significantly reduced the visibility of Tpm and Tn on the surface of F-actin when native TF were used. Small sample volume (~1.8 µL) and fast blotting times (~3 sec) yielded frozen hydrated native TFs possessing well defined Tn densities (Fig. 1A, black arrows). Since the blotting conditions did not affect the integrity of the CL-TFs, we used short blotting times to obtain cryoEM images of both native and cross-linked frozen hydrated TFs under either *relaxing* (pCa>8) or *activating* (pCa=4) conditions (Fig. 1A, insert shows examples of segments used in the image analysis). In the cross-linking experiment TFs were retained in the buffer with low (pCa>8) or high (pCa=4) Ca^{2+} levels before incubation with glutaraldehyde.

Cryo EM image analysis. We used 597 (pCa>8) and 436 (pCa=4) micrographs of native TF along with 1,261 (pCa>8) and 1,762 (pCa=4) of CL-TF possessing a defocus range from 0.5 to 3.5 µm at a raster of 1.05 Å per pixel. Initial correction for the contrast transfer function (CTF) was made by multiplying each image by its theoretical CTF. From these CTF-corrected images we extracted the following number of overlapping (each 460 pixels long) segments: n=31,060 (native TFs, pCa>8), n=9,075 (native TFs, pCa=4), n=41,448 (CL-TF, pCa>8), and n=44,997 (CL-TF pCa=4). Four model volumes were created: pure F-actin (1), TF in the “Blocked” state (2), TF in the “Apo” state (3) and TF in the “Myosin” (4) state. These volumes were scaled to 4.2 Å per pixel and projected onto 115 × 115 px images with an azimuthal rotational increment of 4°, generating 360 reference projections (4 × 90). Segments extracted

from the native or CL-TF at either *relaxing* or *activating* conditions were down-sampled to 4.2 Å per pixel and cross-correlated with 360 reference projections (Fig. 1B). Structural classes were reconstructed with the IHRSR method (5) starting from a solid cylinder as a starting model to yield the following solutions. *Native TF (pCa=4)*: Segments of images that had the best correlation with the pure F-actin model (n=949) were discarded, while the two structural classes yielded a symmetry of: -166,7°/27.2 Å for “c-Closed” set (n=4,535), and -166,6°/27.1 Å for “c-Open” set (n=3,621). The “c-Blocked” class (n=919) did not yield a meaningful 3D-reconstruction (Fig. S3A, black X) and was discarded. *Native TF (pCa>8)*: Segments yielded the best correlation with the pure F-actin model (n=9,332) were discarded, while the three structural classes yielded a symmetry of: -166,8°/27.7 Å for “c-Blocked” set (n=3,809); -166,8°/27.4 Å for “c-Closed” set (n=12,356); -166,7°/27.4 Å for “c-Open” set (n=5,563). *CL-TF (pCa=4)*: Segments of images as being pure F-actin (n=4,531) were discarded, while the three structural classes yielded a symmetry of: -166,0°/27.4 Å for “c-Blocked” set (n=6,977); -166,3°/27.5 Å for “c-Closed” set (n=19,418); -166,3°/27.4 Å for “c-Open” set (n=18,602). *CL-TF (pCa=4)*. Segments selected as being poorly occupied with Tm and Tn (n=4,531) were discarded, while the three structural classes yielded a symmetry of: -166,0°/27.4 Å for “c-Blocked” set (n=6,977); -166,3°/27.5 Å for “c-Closed” set (n=19,418); -166,3°/27.4 Å for “c-Open” set (n=18,602). *CL-TF (pCa>8)*: Segments of images that yielded the best correlation with the F-actin model (n=3,499) were discarded, while the three structural classes yielded a symmetry of: -166,3°/27.4 Å for “c-Blocked” set (n=7,799); -166,4°/27.4 Å for “c-Closed” set (n=19,707); -166,4°/27.4 Å for “c-Open” set (n=9,998). The combined “c-Closed” (n=16,891) and “c-Open” (n=9,184) sets of native TFs converged to the same symmetry of -166,7°/27.3 Å. While the combined “c-Closed” (n=39,125) and “c-Open” (n=28,600) sets of CL-TFs yielded symmetries of -166,4°/27.5 Å and -166,3°/27.5 Å, respectively. The volumes were corrected for the CTF by using a Wiener filter assuming that the signal-to-noise ratio in the

volume was very large. Negative B-factors of 600-900 were used to amplify high frequencies in the reconstruction that were damped by the envelope function of the microscope.

Stopped-flow Measurements of product dissociation from myosin-ADP-Pi by TFs was measured using double mixing stopped-flow fluorescence as described previously (29). Myosin-A1S1 was first mixed with 3 µM of 2'-deoxy-3'mantdATP (mdATP) and incubated in a delay line for 2 s to allow mdATP to bind to the myosin S1 and be hydrolyzed to form the steady state intermediates (M-mdATP” M-mdADP-Pi). The second mix was with either F-actin or TFs. The ratio of mixing was 2:2:5; myosin-S1:mdADP:(MgATP; F-actin or TFs). In experiments designed to minimize rigor activation by myosin heads excess MgATP was included with the TF or F-actin to rapidly dissociate any rigor myosin heads formed by the dissociation of products from the M-mdADP-Pi. In these experiments, the ratio of myosin heads at 50 uM F-actin or TF derived from the myosin-S1 is 1:50 and the rigor myosin heads would be ~90 percent dissociated by the MgATP. It is estimated that there would be less than one rigor myosin-S1 bound to 500 actin subunits at the highest TF concentrations used. .In experiments (identified as "+rigor" in Fig. S2 and S3) where rigor-bound myosin heads were desired, myosin-S1 in excess to the concentration of mdATP was included in the first mix so that 1 in 7 of the actin subunits in the TF will have bound rigor myosin-S1. In these experiments, excess MgATP was not included with the TF. The rate of product dissociation from actomyosin-ADP-Pi is ordered with phosphate dissociation preceding ADP dissociation. In myosin from striated muscle, phosphate dissociation is slower than ADP dissociation and the rate of ADP dissociation (measured here by the decrease in the fluorescence of mdADP) can be used to measure the rate of phosphate dissociation, which limits the rate of force development by cross bridges. The rate constants of product dissociation were determined by fitting the decrease in fluorescence associated with mdADP dissociation from the active

site of myosin to either one or two exponential terms. The faster term is the result of F-actin or TF binding to and accelerating Pi dissociation from M-mdADP-Pi and the slower component for products derived from M-md-ATP.

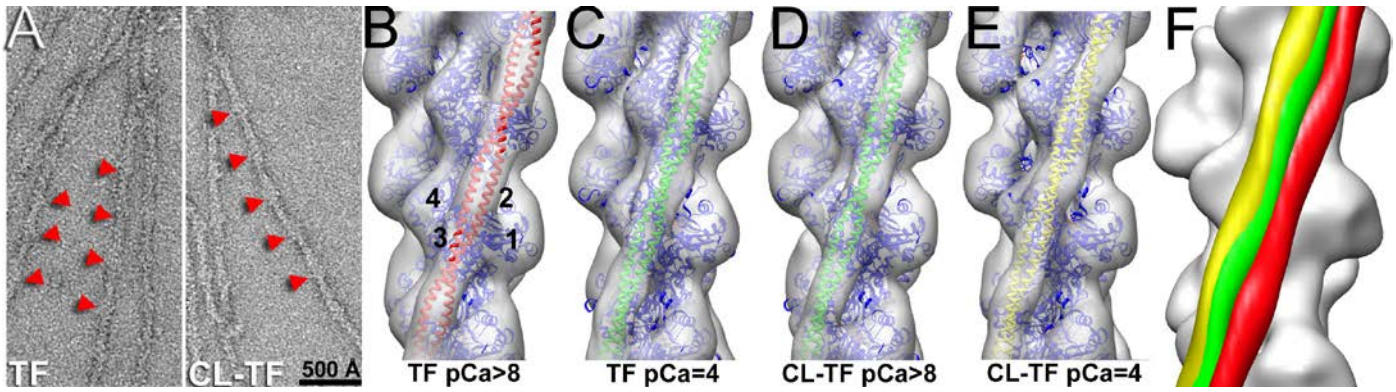

Figure S1. Ca^{2+}-dependent activation of the native cardiac TFs revealed by negative staining. (A) Electron micrographs of native and cross-linked (CL) negatively stained cardiac TFs (pCa>8) show well-defined Tn lumps (red arrowheads). (B and C) 3D-reconstructions of negatively stained native cardiac TF at low (pCa>8) and high (pCa=4) Ca^{2+} show the movement of the Tpm from the “canonical Blocked” (B, red ribbons) to the “Closed” (C, green ribbons) structural state. (D and E) 3D-reconstructions of negatively stained cross-linked (CL) cardiac TFs at low (pCa>8) and high (pCa=4) Ca^{2+} show the movement of Tpm from “Closed” (D, green ribbons) leftward to a structural state which is similar to the “c-Open” structural state of Tpm obtained by cryo EM (E, yellow ribbons). (F) The three positions of Tpm found in the native and cross-linked (CL) TFs are shown in red, green and yellow surfaces using the same color code as in B, D and E, respectively. F-actin is shown in grey. (B-E) 3D-reconstructions are shown as transparent grey surfaces. Atomic model of the actin filament is shown in blue ribbons.

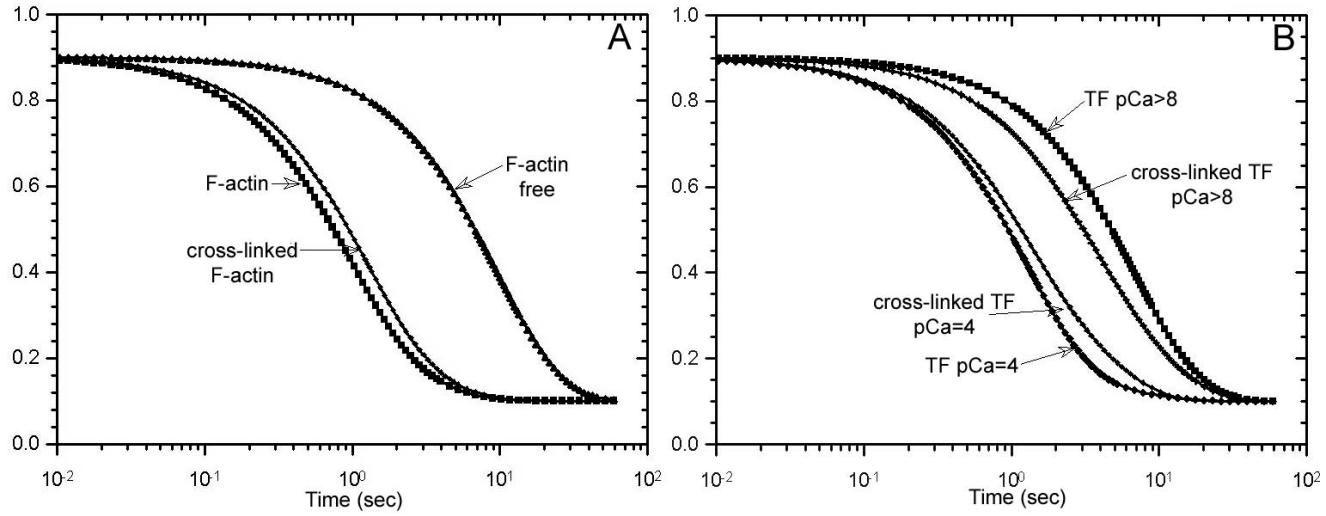

Figure S2. The effect of glutaraldehyde cross-linking on the rate of dissociation of mdADP and Pi from TF-myosin-S1-mdADP-P and F-actin-myosin-S1-mdADP-P at pCa=4 and pCa>8. The rates of product dissociation were measured using double mixing stopped-flow as described in SI methods using experimental conditions similar to those used for preparing samples for cryo-EM 5 mM MOPS, pH 7, 2 mM $MgCl_2$, 1 mM DTT, 50 mM KAc, 1 mM MgATP. Temperature: 20 °C. Initial concentrations were 4 µM A1-S1, 3 µM mdATP, and 6.1 µM TG which produces final concentrations in the flow cell of 0.88 µM myosin-S1, 0.67 µM MgmdATP, 0.67 mM MgATP, and 3.3 µM of either F-actin or TFs. (A) In the absence of actin the rate of dissociation is fit by a single exponential equation with a rate constant of 0.1 s^{-1}. In the presence of 6 uM F-actin the rate of dissociation of mdADP from TF-myosin-S1-mdADP-P is fit by two exponential terms $A(t) = 0.124e^{-1.20t} + 0.0334e^{-.331t}$. Glutaraldehyde cross-linking of F-actin produces a very modest decrease in the acceleration of the product dissociation by decreasing the rates of both exponential terms, which is partially balanced by a slight shift of the amplitudes to the slow phase $I(t) = 0.136e^{-1.12t} + 0.0206e^{-0.231t}$. (B) At pCa =4 the kinetics of product dissociation produced by TF are fit by two rate constants that are similar to those observed with F-actin: $I(t) = 0.141e^{-1.11t} + .0285e^{-0.317t}$

+ C. Crosslinking at pCa=4 increases the rates of both the slow and fast phases but the amplitudes larger: $A(t) = 0.0346e^{-2.5t} + 0.125e^{-0.43t} + C$. At pCa >8 the acceleration of product dissociation also has a slow and fast phase with the amplitude of the slow phase being dominant $I(t) = 0.0087e^{-0.85t} + 0.157e^{-0.134t} + C$. Crosslinking at pCa>8 only produces modest changes in the rates but the amplitude of the fast phase is increased: $I(t) = 0.026e^{-0.94t} + 0.136e^{-0.175t} + C$. Overall glutaraldehyde crosslinking slightly reduces the overall rate of product dissociation at pCa=4 and slightly increases the rate at pCa>8 by making small changes in the rates and amplitudes.

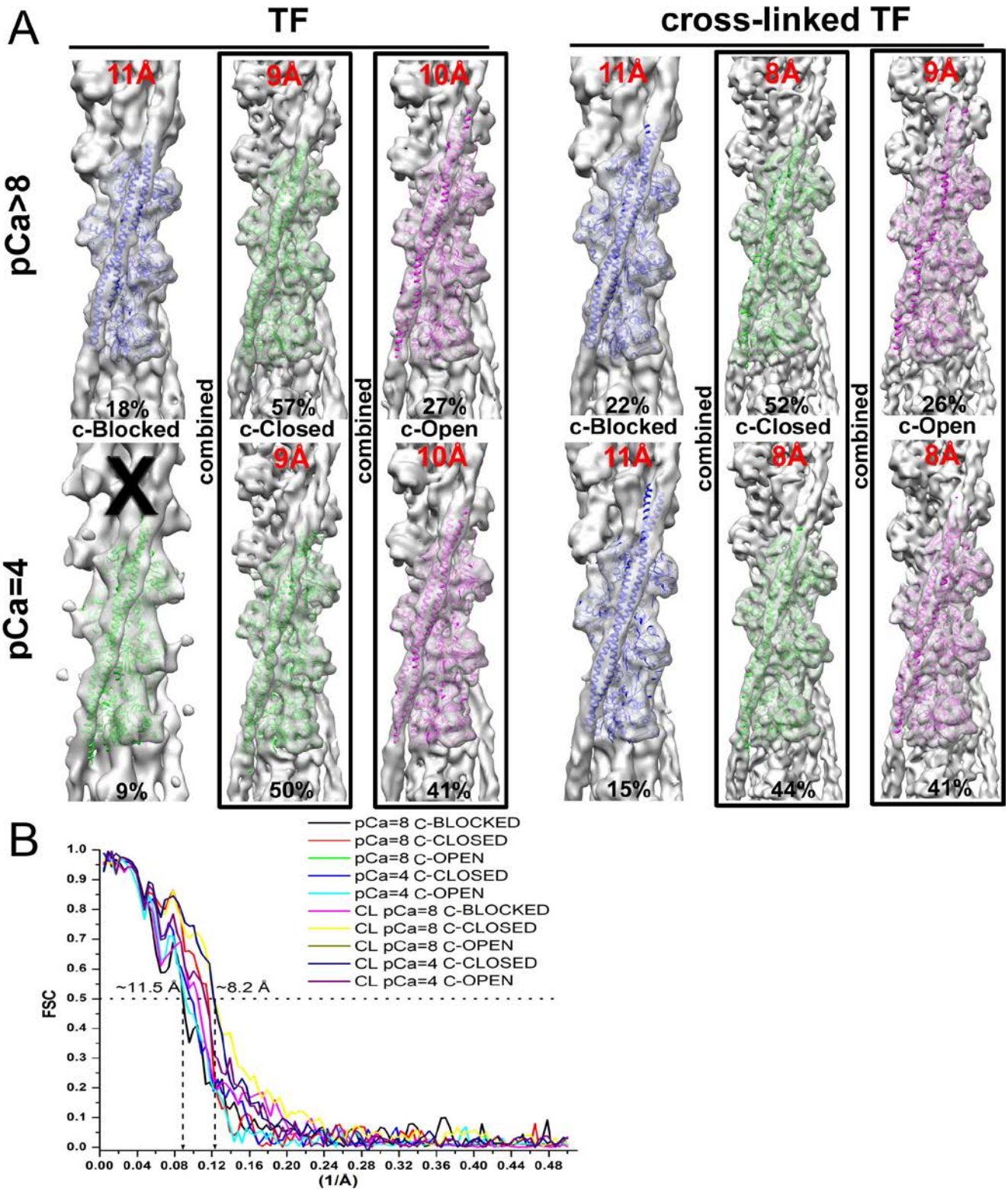

Figure S3. (A) 3D-reconstructions of structural classes yielded by cross-correlation sorting of native cardiac TFs (Fig. 1B, left panel) were obtained using IHRSR approach (5). Actual

density maps are shown as transparent grey surfaces, while corresponding pseudo-atomic models docked into the maps using DirX software (6) for “c-Blocked”, “c-Closed” and “c-Open” structural states are shown as blue, green and magenta ribbons, respectively. Frequency of each structural state is denoted at the bottom in black, while resolution determined for each class using FSC method (shown in C) is denoted in red. 3D-reconstruction of the “c-Blocked” structural state that possesses Tpm in the “c-Closed” structural state is marked with a black “X”. (B) 3D-reconstructions of structural classes yielded by cross-correlation sorting of cross-linked cardiac TFs (Fig. 1B, right panel) were obtained using IHRSR approach (5). Actual density maps are shown as transparent grey surfaces, while corresponding pseudo-atomic models docked into the maps using DirX software (6) for “c-Blocked”, “c-Closed” and “c-Open” structural states are shown as blue, green and magenta ribbons, respectively. (C) 0.5 FSC criterion was used to determine resolution of each individual structural class. Each class was split into two non-overlapping halves and independent 3D-reconstruction of each half was independently calculated using IHRSR approach (5). Due to the reduction of the number of particles in each half, this approach yields the most pessimistic estimation of resolution.

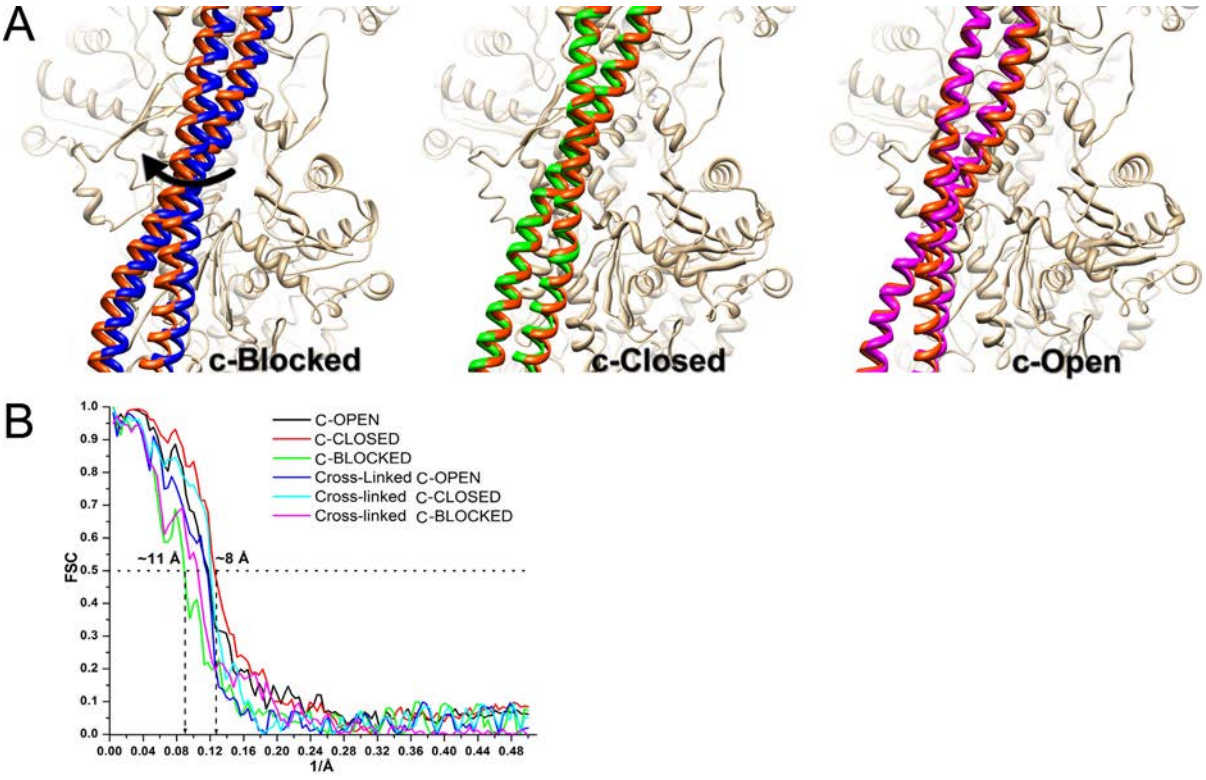

Figure S4. (A) Comparison of the positions of Tpm in the pseudo-atomic models obtained from the 3D-reconstructions of the “c-Blocked”, “c-Closed” and “c-Open” structural states of the native (Fig. 1C) and cross-linked (Fig. 1D) TFs. Actin molecules are in tan. Tpm in the “c-Blocked”, “c-Closed” and “c-Open” structural states of native cardiac TFs is shown in blue, green and magenta, respectively. Tpm from the three structural states obtained from the cross-linked TFs is in orange. The swing of Tpm upon cross-linking in the “c-Blocked” structural state is marked with a black arrow. (B) 0.5 FSC criterion was used to determine resolution of each individual structural class shown in Figure 1C and D. Each class was split into two non-overlapping halves and 3D-reconstruction of each half was independently calculated using IHRSR approach (5). Due to the reduction of the number of particles in each half, this approach yields the most pessimistic estimation of resolution.

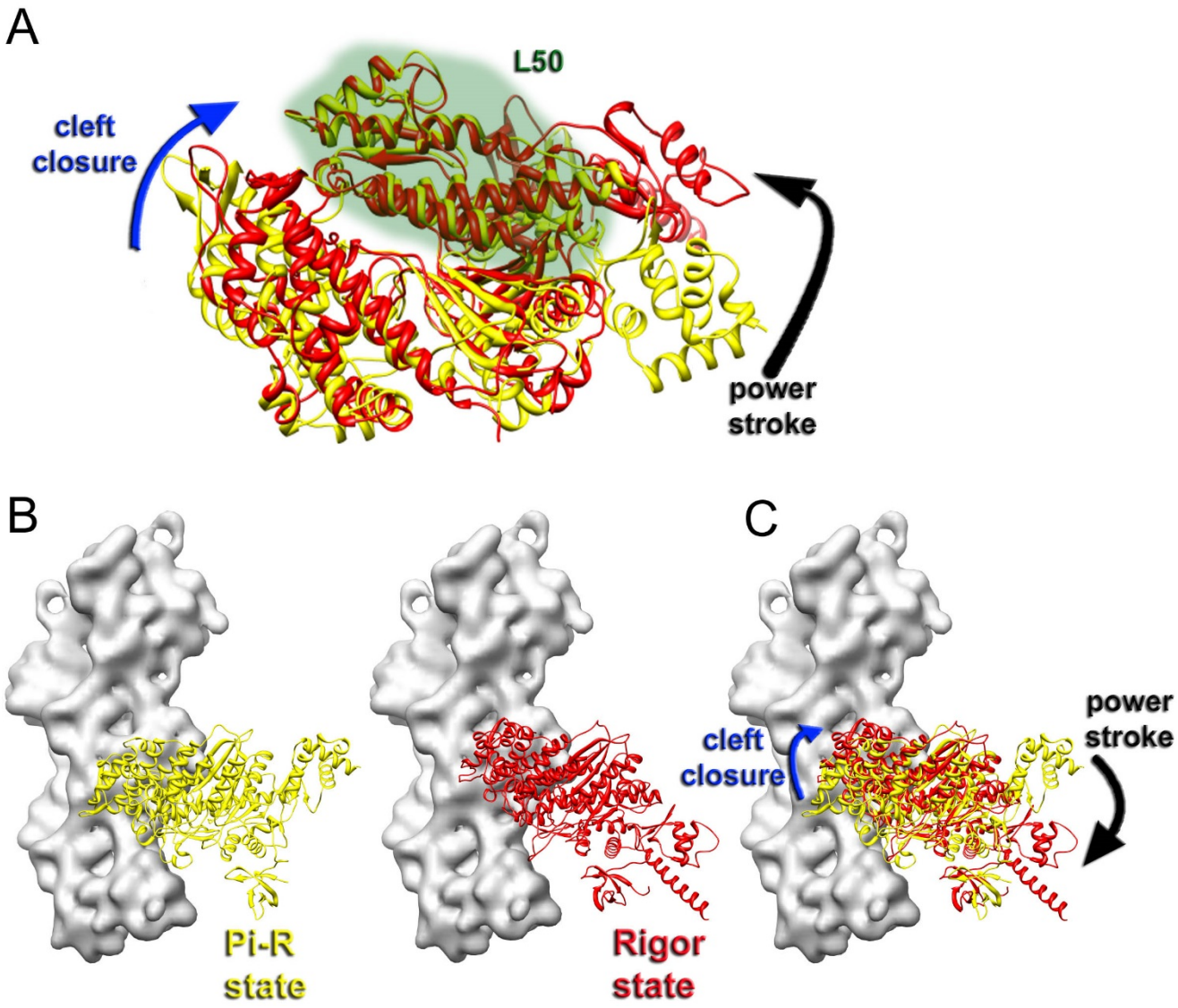

Figure S5. (A) In order to approximate the initial strong binding mode of myosin, we used the same approach described by von der Ecken et al. (7). The LP50 domain of myosin the head from the crystal structure of the myosin P_i-release state (P_i-R state, yellow ribbons) (PDB accession number 4PFO) (8) was aligned to the L50 domain of rigor bound myosin (red ribbons) (PDB accession number 5JLF) (7). The region of alignment is outlined in transparent green. The two major differences between the P_i-R and rigor state of myosin include cleft closure (blue arrow) and rotation of the swivel arm upon power stroke (black arrow). (B) Myosin position on the surface of F-actin (grey surface) is shown in yellow for P_i-R state and in red for rigor bound myosin. (C) The two modes of myosin binding are aligned on the

surface of F-actin. The direction of the cleft closure is marked with a blue arrow, while the rotation of the swivel arm of myosin upon the power stroke is denoted by a black arrow.

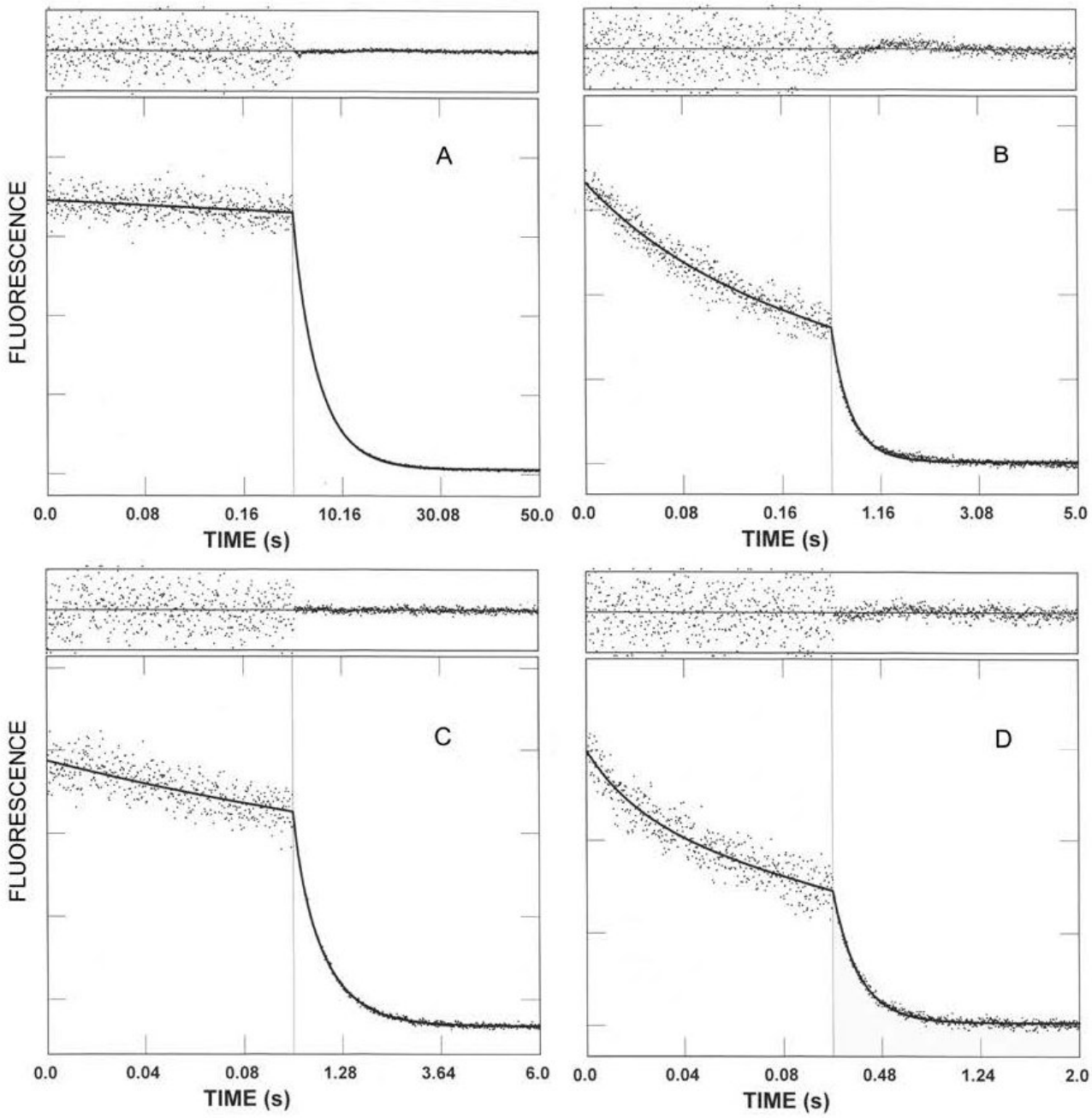

Figure S6. Effect of Ca^{2+} and rigor myosin-S1 on the acceleration of product dissociation from myosin-S1-mdADP-Pi by cardiac TF at near physiological ionic strength. Double mixing stopped-flow experiments were performed as described in SI Materials and Methods. (A and B - no rigor activation): 2 μM A1S1 and 3 μM mdATP were mixed, incubated for 1 second and then mixed with 40 μM (actin subunit concentration)

cardiac thin filaments containing 1 mM MgATP and either 1.0 mM EGTA (A) or 0.2 mM $CaCl_2$ (B). Final concentrations in the flow cell: 0.44 µM cardiac S1, 0.66 µM md-nucleotide, 22.2 µM cardiac thin filaments, 0.55 mM ATP, 2 mM $MgCl_2$, 5 mM MOPS, 100 mM KAc and either 0.55 mM EGTA (A) or 0.1 mM $CaCl_2$ (B), pH 7, 20^o C. (C and D + rigor activation): 16 µM of cardiac S1 and 2 µM mdATP were mixed, incubated for 1 second and then mixed with cardiac thin filaments containing either 1.0 mM EGTA (C) or 0.1 mM $CaCl_2$ (D). Final concentrations in the flow cell: 3.55 µM myosin-S1, 0.44 µM md-nucleotide, 21.5 µM cardiac thin filaments, 3.1 µM myosin-A1-S1 bound to TF, 2 mM $MgCl_2$, 5 mM MOPS, 100 mM KAc and either 0.55 mM EGTA (C) or 0.1 mM $CaCl_2$ (D), pH 7, 20^o C. The solid lines through the data are the best fits to the following exponential equations: (A) $I(t) = 0.06e^{-0.79t} + 0.6e^{-0.19t} + C$; (B) $I(t) = 0.14e^{-6.2t} + 0.50e^{-1.3t} + C$; (C) $I(t) = 0.17e^{-11.1t} + 0.50e^{-2.5t} + C$; (D) $I(t) = 0.12e^{-51t} + 0.47e^{-5.0t} + C$.

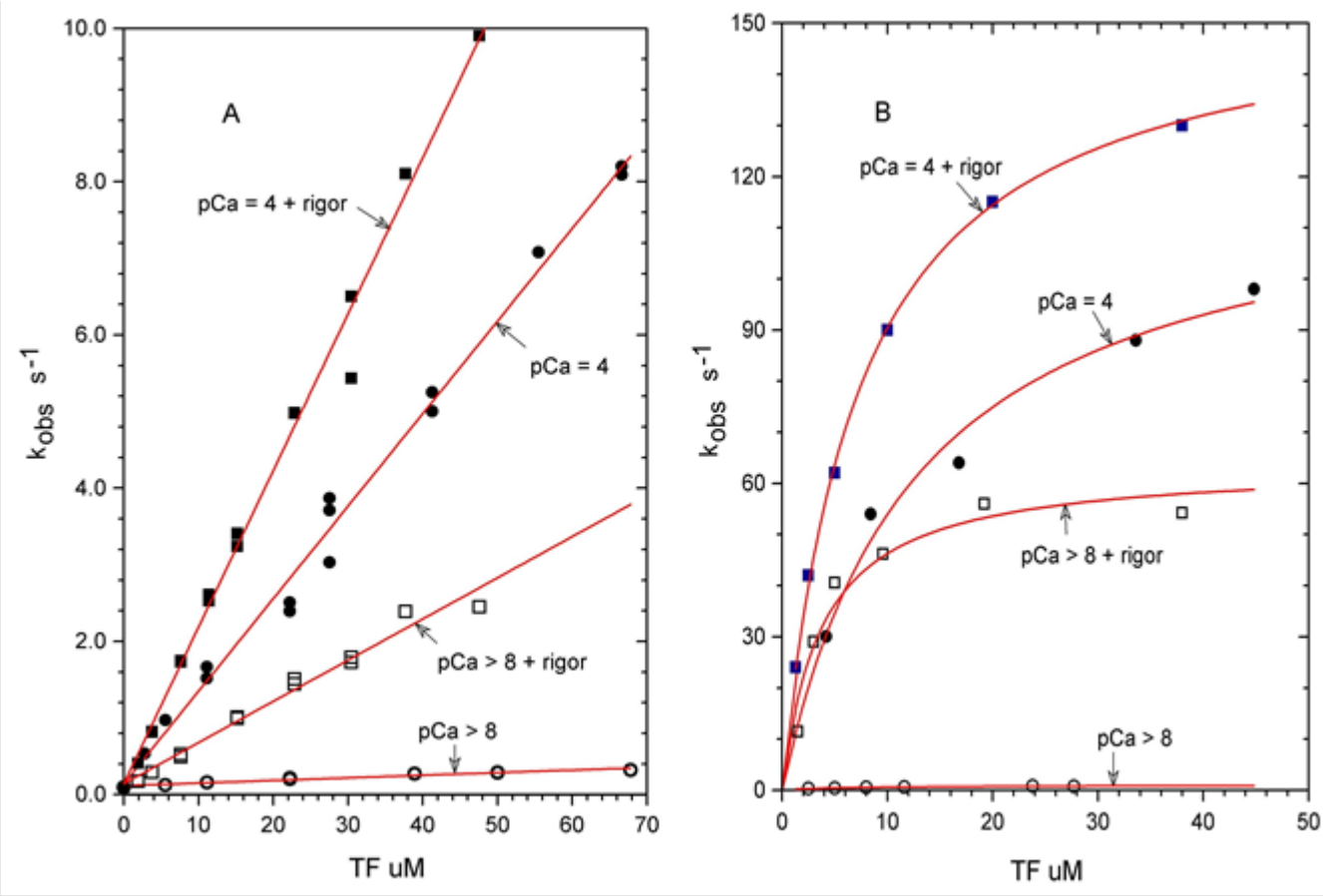

Figure S7 Dependence of the rates of product dissociation from myosin-S1-mdADP-Pi on cardiac TF concentration, Ca^{+2}, and rigor myosin-S1 bound to the TF. Double mixing experiments were carried out in either 5 mM MOPS, 2 mM $MgCl_2$, 100 mM KAc, pH 7, 20° (A) or in the same buffer with 22 mM KAc (B) and either 0.2 mM $CaCl_2$ (pCa=4) or 1 mM EGTA (pCa > 8). In experiments identified as "+rigor" (and ¡) there was one molecule of apo A1S1 in the flow cell per seven actin subunits in the TF. Experiments not so designated contained 0.55 mM MgATP in the flow cell to rapidly dissociate any rigor A1-S1 bound to the TF. (A) The effect of rigor myosin-S1 and Ca^{2+} on the values for k_{-P}/K_{TF} were obtained from the slope of a linear fit: $k_{obs.} = k_{-P}[TF]/K_{TF}$. (B) The effect of rigor myosin and Ca^{2+} on the parameters k_{-P} and K_{TF} were obtained by fitting the data to a hyperbolic equation, $k_{obs} = k_{-P} / (1 + K_{TF}/[TF])$, which is consistent with a two-step mechanism in which an initial binding step

precedes rate limiting phosphate dissociation (TF + M-mdADP-Pi ” TF-M-mdADP-Pi ’ TF-M-mdADP + Pi). The values for k_{-P}, K_{TF}, and k_{-P}/K_{TF} are summarized in Table ST1.

Table ST 1. Summary of the Effect of Rigor Myosin-S1 and Ca^{2+} Binding to CardiacTF on the Kinetics of Product Dissociation.

	[KAc]				
pCa		>8	>8	4	4
Rigor (1 myosin-S1/actin)		-	+	-	+
k_{-p} (s^{-1})	22	0.9 (±.1)	64 (±4)	122 (±6)	155(±5)
K_{TF} (μM)	22	5.8 (±2)	3.8 (±1)	12.7 (±2)	7.1(±0.6)
Percent Activation k_{-p}/k_{max}	22	0.7	41	79	100
k_{-p}/K_{TF} (μM^{-1} s^{-1})	100	0.0019(±0.0002)	0.057(±0.004)	0.13(±0.01)	0.18(±0.01)
Percent Activation: k_{-p}/K_{TF} (μM^{-1} s^{-1})/ k_{-p}/K_{TF} (μM^{-1} s^{-1})max	100	1	31	72	100

Values for k_{-p}/K_{TF} from fits to the data in Fig. S7 (A) in 100 mM KAc and for and k_{-p} were obtained from the data in Fig. S7 (B) at 22 mK KAc using the Scientist fitting software. Values in parenthesis are standard errors.

Figure S7A shows the dependence of the rate of Pi dissociation at a salt concentration approaching physiological values (100 mM KAc) where the dependence of rate on [TF] is linear and it is no longer possible to separately determine k_{-P} and $K_{TF.}$ The slope is a measurement of the second order rate constant, k_{-P}/K_{TF}, of (myosinA1S1-mdADP-Pi +TF ” TF-myosinA1S1-mdADP-Pi ’ TF-myosinA1S1-mdADP + Pi). The percent activation are calculated relative to the maximum activation obtained in the presence of one rigor myosin head per 7 actin subunits at pCa = 4.

Figure S7B shows the effect of calcium and rigor bound myosin-A1S1 on the rate of Pi dissociation at the highest salt concentration (22 mM KAc) that it is feasible to separately determine the rate of Pi dissociation, k_{-P} at saturating concentrations of TF and $K_{TF,}$ the dissociation constant of M-ADP-Pi from TF-M-ADP-Pi. The fit values for the rates k_{-P} and K_{TF} are shown in Table S1T. The dependence of the values for the percent activation of k_{-P} at 22 mM KAc shows a similar effect of the ligands Ca^{2+} and rigor S1 as determined for k_{-P}/K_{TF} at

100 mM KAc: pCa=4 + rigor > pCa=4 > pCa>8 + rigor > pCa>8. Although neither calcium nor rigor myosin alone can maximally activate cardiac TF, the acceleration of product dissociation at pCa=4 produces >70% maximal activation and rigor myosin produces only a relatively small additional increase. These results are not consistent with the classic steric blocking mechanism, which predicts that rigor myosin is required to activate the thin filament in the presence and absence of Ca^{+2}. Moreover, the results obtained here are quantitatively different than those obtained with reconstituted skeletal muscle TFs (9), where rigor myosin-S1 increased the rate of phosphate dissociation at pCa=4 by 5-fold.

Supplementary movie 1. Trajectory of Tpm movement on the surface of F-actin. Movie starts from the transition of the “c-Blocked” (blue) into the “c-Closed” state (green), followed by transition of the “c-Closed” (green) into the “c-Open” (magenta) state. Finally, transition of “c-Open” state into the “Myosin” state (cyan) completes the Tpm swing on F-actin.

Supplementary movie 2. Trajectory of Tpm movement on the surface of F-actin (Movie S1) is superimposed on the atomic model of rigor myosin-F-actin complex. (7). Sterical clashes between myosin head and Tpm in the “c-Blocked” (blue) and the “c-Closed” (green) structural states are marked with big yellow arrows, while a small sterical hindrance between loop-4 of myosin and Tpm in the “c-Open” structural state is indicated with small yellow arrow.

.

Reference List

1. **Galkin, V. E., Orlova, A., Vos, M. R., Schroder, G. F., & Egelman, E. H. (2015) Near-atomic resolution for one state of f-actin. Structure. 23:173-182.**

2. **Li, X. E., Tobacman, L. S., Mun, J. Y., Craig, R., Fischer, S., & Lehman, W. (2011) Tropomyosin position on F-actin revealed by EM reconstruction and computational chemistry. Biophys. J. 100:1005-1013.**

3. **von der, E. J., Muller, M., Lehman, W., Manstein, D. J., Penczek, P. A., & Raunser, S. (2015) Structure of the F-actin-tropomyosin complex. Nature 519:114-117.**

4. **Behrmann, E., Muller, M., Penczek, P. A., Mannherz, H. G., Manstein, D. J., & Raunser, S. (2012) Structure of the rigor actin-tropomyosin-myosin complex. Cell 150:327-338.**

5. **Egelman, E. H. (2000) A robust algorithm for the reconstruction of helical filaments using single-particle methods. Ultramicroscopy 85:225-234.**

6. **Schroder, G. F., Brunger, A. T., & Levitt, M. (2007) Combining efficient conformational sampling with a deformable elastic network model facilitates structure refinement at low resolution. Structure. 15:1630-1641.**

7. **von der, E. J., Heissler, S. M., Pathan-Chhatbar, S., Manstein, D. J., & Raunser, S. (2016) Cryo-EM structure of a human cytoplasmic actomyosin complex at near-atomic resolution. Nature 534:724-728.**

8. **Llinas, P., Isabet, T., Song, L., Ropars, V., Zong, B., Benisty, H., Sirigu, S., Morris, C., Kikuti, C., Safer, D. *et al.* (2015) How actin initiates the motor activity of Myosin. Dev. Cell 33:401-412.**

9. **Heeley, D. H., Belknap, B., & White, H. D. (2002) Mechanism of regulation of phosphate dissociation from actomyosin-ADP-Pi by thin filament proteins. Proc. Natl. Acad. Sci. U. S. A 99:16731-16736.**